Stability-Oriented Adaptive Synchronization Control for Networked Microgrids

Basati, Amir; Guan, Yajuan; Bazmohammadi, Najmeh; Vasquez, Juan C.; Guerrero, Josep M.

Published in:
IEEE Transactions on Industry Applications

DOI (link to publication from Publisher):
10.1109/TIA.2026.3654503

Publication date:
2026

Document Version
Accepted author manuscript, peer reviewed version

Stability-Oriented Adaptive Synchronization Control for Networked Microgrids

Amir Basati, *Member, IEEE,* Yajuan Guan, *Member, IEEE,* Najmeh Bazmohammadi, *Senior Member, IEEE,* Juan C.Vasquez, *Senior Member, IEEE,* and Josep M. Guerrero, *Fellow, IEEE*

***Abstract*—This paper presents an adaptive synchronization control mechanism (ASCM) using an online ridge regression strategy for networked AC microgrids (ACMGs). The understudied ACMG system comprises multiple voltage source inverters (VSIs), where the proposed adaptive mechanism is utilized to dynamically tune the controllers' gain in real-time. This adaptive synchronization layer improves the performance of the control system in transient conditions, such as abrupt load fluctuations, plug-and-play (PnP) operations and maintains the robust operation in the presence of measurement noise and communication disturbances, all without imposing a significant additional computational burden. Moreover, the stability of the closed-loop system is ensured through a Lyapunov-based analysis, ensuring bounded tracking error and robustness to parameter uncertainties. The simulation results in MATLAB/Simulink show that the proposed decentralized secondary control achieves a 75% improvement in response time to rapid reference changes, reducing it from 2 seconds with centralized secondary control to 0.5 seconds, while also improving voltage tracking performance. It also significantly reduces frequency deviations during PnP events (∼10×), representing a substantial improvement compared to conventional fixed-gain secondary controllers commonly used in networked ACMGs.**

***Index Terms*—Networked AC Microgrids, Adaptive Synchronization Mechanism, Ridge Regression, Voltage Source Inverter, Plug-and-Play Functionality.**

I. Introduction

THE global transition toward renewable energy is reshaping our current power systems by allowing greater integration of distributed energy resources (DERs) such as photovoltaics, wind turbines, battery storage systems, etc. Among the most promising solutions for resilient and sustainable power supply, microgrids (MGs) show that they can be one of the most efficient solutions, facilitating local integration of renewable energy sources (RESs) and providing flexible operation in both grid-connected and islanded modes. This is particularly beneficial for remote regions and weak-grid conditions, where centralized power distribution remains infeasible or unreliable. MGs have emerged as a viable solution to address the challenges by supplying uninterruptible power to critical loads, due to their operational flexibility and controllability. However, the widespread deployment of inverter-based DERs has introduced new challenges, particularly concerning system stability, dynamic performance, and control coordination in networked AC microgrid (ACMG) systems. One of the core issues arises from the reduction of physical inertia in inverter-dominated systems, making power systems more sensitive to frequency and voltage disturbances, especially under high penetration of intermittent RESs [1]. Therefore, efficient methods must be devised to integrate RESs into the power system to prevent disturbances and frequent blackouts. In cases where (a) high energy generation capacity, (b) enhanced overall system resilience, (c) scalability, and (d) operational flexibility are required, a single MG may not provide an effective solution. In such situations, employing multi-microgrid systems that interconnect several MGs can significantly enhance power system resilience. However, this approach also introduces added complexity in control and operation management, including coordinated energy management, stable operation, dynamic response, and disturbance rejection across the interconnected MGs. Therefore, a well-designed control system is needed to ensure the resilience, reliability, and stability of ACMG systems, which is the main reason why they have been the subject of significant focus in recent years. Among the various types of control structures, the hierarchical control scheme has gained more attention from scientific and industrial specialists. Conventional hierarchical control structures consist of three levels: primary, secondary, and tertiary [2]. The hierarchical control structures, due to their powerful multi-timescale property, are widely used in ACMGs because they effectively manage the state of charge, load current sharing, and restoration of the bus voltage. However, dependence on a communication network also exposes the system to cyberattacks [3], [4], which has led to increased interest in developing robust attack detection algorithms for MGs with hierarchical control systems [5]. Although decentralized primary droop-based controllers are common, the majority of hierarchical control architectures employ centralized secondary and tertiary control layers [6]. In addition, centralized control approaches often face scalability issues, especially in large-scale or highly distributed systems, where communication delays and single point of failures can limit overall system reliability and flexibility.

In a hierarchical control system, the control signal for the secondary controller is highly dependent on the data received from the connected neighboring units; therefore, data precision is crucial to attaining the intended control objective for the hierarchical control structure in ACMGs. Furthermore, a fundamental challenge in control lies in guaranteeing smooth and robust synchronization among the interconnected MGs, especially under plug-and-play (PnP) conditions and during

Amir Basati, Yajuan Guan, Najmeh Bazmohammadi, Juan C. Vasquez and Josep M. Guerrero are with the Center for Research on Microgrids (CROM), AAU Energy, Aalborg University, Aalborg, Denmark (e-mail: {amba, ygu, naj, juq, joz}@energy.aau.dk). Josep M. Guerrero is also with the Department of Electrical Engineering of Valladolid University, Valladolid, Spain. (Corresponding author: Amir Basati.)

abrupt changes. Standard control loops for synchronization often utilize phase-locked loops (PLLs) with fixed gain, which may not provide the necessary adaptability to the synchronization problem in a poorly conditioned structure that acts like a weak grid [7].

To address the abovementioned problems, this paper proposes an Adaptive Synchronization Control Mechanism (ASCM) based on the previously introduced decentralized secondary control architecture in [8]. The proposed decentralized methodology includes an online learning strategy for adaptive synchronization among interconnected MGs. This online mechanism is based on ridge regression and acts as a Bayesian update for the loop gain of the synchronization control law. Simulation studies evaluate the controller's performance under various conditions, including reference voltage tracking, PnP operations, abrupt load disturbances, measurement noise, and impaired communication. The main contributions of this work can be summarized as follows:

- An ASCM is developed using an online ridge regression technique, enabling real-time adaptive tuning of synchronization gains within a decentralized secondary control framework, without requiring offline tuning or central coordination.
- The proposed control layer improves transient stability and frequency tracking performance without increasing computational burden.
- The stability of the proposed framework is analyzed and ensured through a Lyapunov-based stability analysis.

The rest of this paper is organized as follows. Section II describes the overall system architecture and the conventional droop-based hierarchical control structure. Section III introduces the proposed Adaptive Synchronization Control Mechanism, including its online learning formulation, computational characteristics, and stability analysis. Section IV presents a detailed simulation study comparing the performance of the proposed approach with conventional fixed-gain secondary controllers under several realistic simulation scenarios. Section V offers a detailed discussion of the observed results and their implications for practical deployment. Finally, Section VI concludes the paper and outlines future research directions.

II. System Architecture and Hierarchical Control Design

A. System Architecture

The overview of the hierarchical control scheme for an networked MG is presented in Fig. 1. The diagram illustrates the connection between two MGs, MG1 and MG2, through distribution lines that link to an AC bus. Each MG unit is made up of two voltage source inverters (VSI) that can represent DERs, such as photovoltaic and hybrid battery systems. It should be noted that the switches SW_{C1}, SW_{C2}, SW_{C3}, and SW_{C4} act as routing elements that determine whether each VSI receives its secondary control signal from the decentralized controller or from the centralized controller. Each switch can pass either the decentralized (a-side) or the centralized (b-side) controller command, but never both simultaneously. In this work, the main focus is on the ASCM employed in such a networked architecture, where synchronization is adaptively maintained through an online ridge regression-based learning mechanism applied at the secondary control level.

B. Droop-based Hierarchical Control

Droop-based hierarchical control strategy is a widely used approach in MG applications [9]. At the primary level, the droop control method is used to regulate the frequency and voltage of the MG. This involves subtracting proportional parts of the average active and reactive power output from the frequency and output voltage of each unit, as follows:

$$\omega = \omega^* - G_P \times (P - P^*) \tag{1}$$

$$E = E^* - G_Q \times (Q - Q^*) \tag{2}$$

The frequency and amplitude of the output voltage reference are denoted by ω and E, respectively, while their respective references are represented by ω^* and E^*. Active and reactive powers are symbolized by P and Q, with references to P^* and Q^*. The two transfer functions, G_P and G_Q, are considered proportional droop terms in the island operation mode in this study, which can be designed to keep the system synchronized within the voltage and frequency deviation limits according to related IEEE standards by controlling the static deviations $\Delta P/\Delta\omega$ and $\Delta Q/\Delta V$, which can be designed as follows [10]:

$$G_P = \Delta\omega/P_{max} \tag{3}$$

$$G_Q = \Delta V/2Q_{max} \tag{4}$$

where P_{max} and Q_{max} are the maximum active and reactive powers supplied by the inverter, respectively, and $\Delta\omega$ and ΔV are the maximum acceptable voltage and frequency deviations that can be tolerated according to the grid codes. The droop control loops, commonly called $P-\omega$ and $Q-E$ droops, are employed, as depicted in Fig. 1.

In a hierarchical control scheme, the secondary control is responsible for coordinated power and energy control, synchronization control, power quality improvement, reactive power sharing improvement, etc. The tertiary control optimizes the performance of the MG by adjusting the set points of the primary and secondary control levels. This approach is highly effective in ensuring the stable operation of MGs, which are increasingly being used as an alternative to conventional centralized control approaches [11].

By utilizing the secondary control, the frequency and amplitude deviations can be compensated. Each time the MG's loads or power generation changes, the secondary control brings the voltage and frequency deviations back into the allowed region. For example, in northern European countries, secondary control is employed to bring the frequency deviation of the grid within the permissible limit of ±0.1 Hz [12]. Typically, conventional controllers, which are also known as load-frequency control schemes, are utilized to keep the system performance within an acceptable range according to related IEEE standards [13]. In contrast to conventional fixed-gain secondary controllers [14], this work introduces an adaptive gain update mechanism that is implemented through

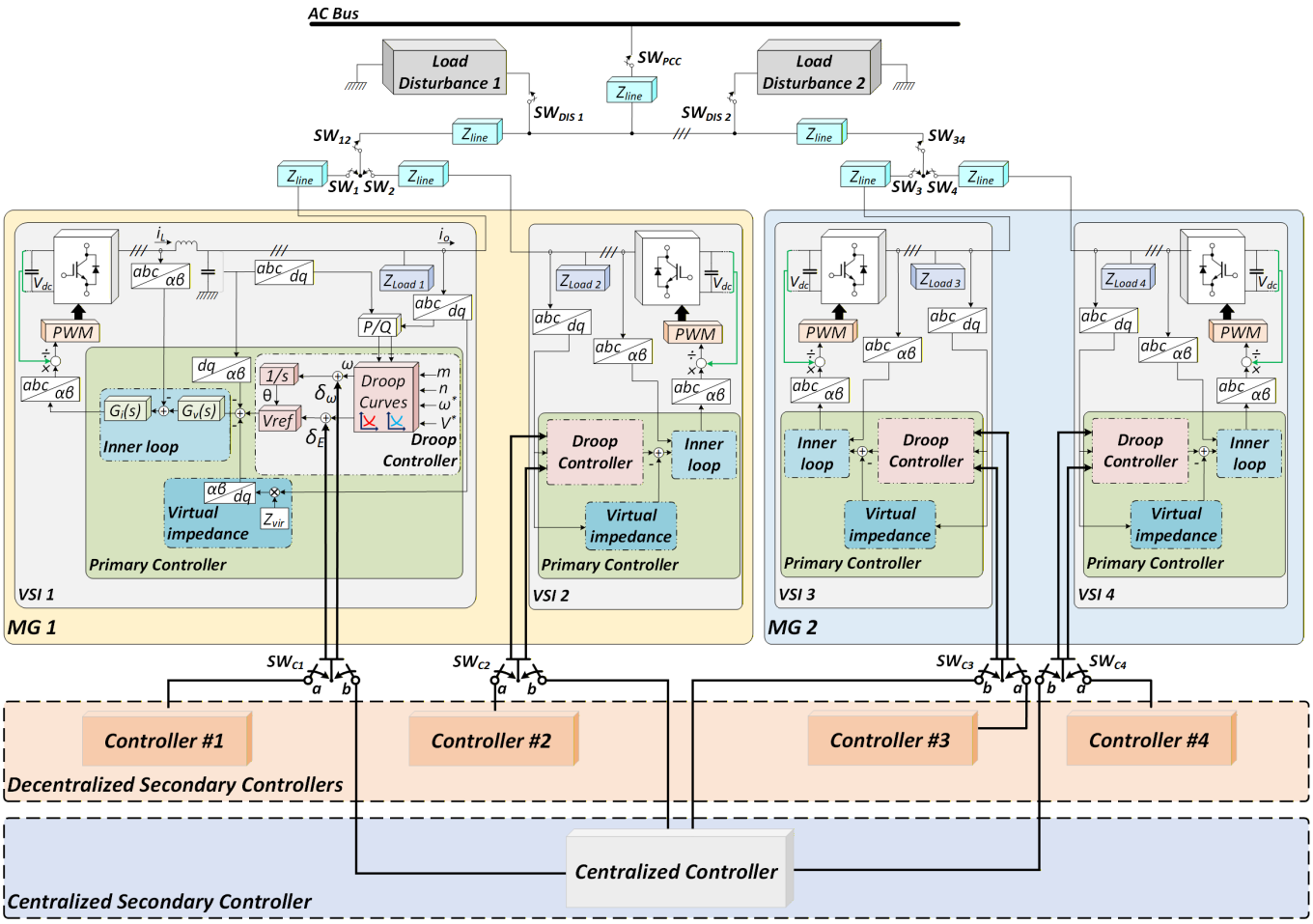

Fig. 1. Understudied Interconnected ACMG System.

online ridge regression. This strategy allows the controller to learn the optimal parameters in real time, improving its robustness to system disturbances and uncertainties.

The control law for frequency and output voltage restoration can be obtained as follows:

$$\delta\omega = K_p^{\omega}(\omega_{MG}^{*} - \omega_{MG}) + K_i^{\omega}\int(\omega_{MG}^{*} - \omega_{MG})dt + \Delta\omega^{*} \tag{5}$$

$$\delta E = K_p^{E}(E_{MG}^{*} - E_{MG}) + K_i^{E}\int(E_{MG}^{*} - E_{MG})dt \tag{6}$$

The control parameters of the secondary control scheme are denoted as K_p^{ω}, K_i^{ω}, K_p^{E}, and K_i^{E}, while the deviation compensation term $\Delta\omega^{*}$ should remain equal to zero when the MG is operated in the islanded mode. The frequency and output voltage of the MG denoted as ω_{MG} and E_{MG}, are measured and compared with the references ω_{MG}^{*} and E_{MG}^{*}. Secondary control units generate appropriate control signals, instructing the primary controller to restore the output voltage frequency and amplitude based on errors processed through compensators, denoted $\delta\omega$ and δE, respectively. Here, $\delta\omega$ and δE must be restricted (according to the grid codes) so that they do not violate the allowed limits for maximum frequency and output voltage deviations [15], [16].

III. Adaptive Synchronization Control and Stability Analysis

A. Adaptive Synchronization Control Mechanism (ASCM)

To enable seamless synchronization among distributed VSIs in interconnected ACMGs, an ASCM is incorporated into the secondary control layer. This control loop is based on the conventional method that computes a synchronization correction frequency ω_{sync} based on the phase misalignment between local VSI voltages (V_{VSI}) and the corresponding MG bus voltages (V_g), both expressed in the α–β stationary frame. The synchronization error signal is derived from the cross product of the two voltage vectors:

$$e(t) = V_g \times V_{VSI} = V_{g-\beta}(t)V_{VSI-\alpha}(t) - V_{g-\alpha}(t)V_{VSI-\beta}(t) \tag{7}$$

where the controller processes the error signal $e(t)$ to compute the control input ω_{sync}, which is then added to the primary droop controller. This frequency term is then used to adjust each VSI's $P-\omega$ droop equation, facilitating coordinated frequency regulation across the system. Although traditional PLLs provide a reliable means of tracking phase and frequency, they typically rely on fixed PI gains, which limit their adaptability under transient or non-linearity in weak grid conditions [17], [18]. The proposed control loop integrates

an online ridge regression algorithm to adaptively tune the synchronization controller parameters. The ridge regression algorithm is a regularized least-squares estimator that stabilizes parameter updates by penalizing large gain values. In its online form, the algorithm updates the parameter vector recursively at each sampling time, using only current measurements and an internal covariance matrix. This formulation avoids storing historical data and ensures bounded, noise-resistant parameter adaptation, which makes it suitable for real-time control tasks where measurement disturbances and modeling uncertainties are present. Therefore, the proposed control loop integrates this online algorithm to adaptively tune the synchronization controller parameters (K_p^{sync} and K_i^{sync}) in real time, as depicted in Fig. 2. The time-varying gains $K_p^{\text{sync}}(t)$ and $K_i^{\text{sync}}(t)$ are updated recursively based on the observed synchronization error, allowing the controller to adapt in real time to changes in load or generation conditions without manual tuning.

The algorithm minimizes a regularized squared prediction error between the observed synchronization behavior and the expected control effort, thereby enabling the controller to dynamically respond to changing operating conditions such as PnP events, abrupt load perturbations, or inverter parameter mismatches (model parameter uncertainties). Therefore, the adaptive control strategy complements the PLL-based methods when advanced synchronization performance is needed. It is important to clarify that the PLL remains responsible for extracting the local voltage phase and frequency in the primary control layer; however, its fixed-gain structure makes it sensitive to weak-grid conditions, measurement noise, and harmonic distortion. The adaptive synchronization controller operates at the secondary layer and generates a correction frequency term based on real-time error trends rather than fixed PI gains. By continuously adapting $K_p^{sync}(t)$ and $K_i^{sync}(t)$ through the online ridge regression update, the controller suppresses phase jumps, improves damping during transients, and reduces the PLL's burden in distorted conditions. In this sense, the adaptive layer enhances the PLL's performance by shaping the overall synchronization dynamics, and in certain specific scenarios, it can provide a more accurate and responsive frequency correction compared to a fixed-gain PLL alone.

The core update rule follows a standard online regularized least-squares formulation. Let $x(t) = [e(t), \int_0^t e(\tau)d\tau]^T$ denote the feature vector formed by the instantaneous synchronization error $e(t)$ and its integral. In addition, $u(t)$ represents the desired control action (i.e., the correction frequency ω_{sync}). The adaptive controller seeks to learn a parameter vector $\boldsymbol{\theta}(t) = [K_p^{\text{sync}}(t), K_i^{\text{sync}}(t)]^T$ by minimizing the instantaneous regularized squared error at each time step:

$$J(t) = \Big(u(t) - \boldsymbol{\theta}^T(t)x(t)\Big)^2 + \lambda\|\boldsymbol{\theta}(t)\|^2 \tag{8}$$

Here, $\lambda > 0$ is the regularization parameter that prevents overfitting and ensures numerical stability [19]. The regularization term $\lambda\|\boldsymbol{\theta}(t)\|^2$ ensures the numerical stability of the gain update process, especially under frequent load changes or noisy voltage measurements. It also prevents parameter drift in long-term operation. The solution is updated recursively using the following online update rule:

$$\boldsymbol{\theta}(t) = \boldsymbol{\theta}(t-1) + \mathbf{K}(t)\Big[u(t) - \boldsymbol{\theta}^T(t-1)x(t)\Big] \tag{9}$$

$$\mathbf{K}(t) = \frac{\mathbf{P}(t-1)x(t)}{1 + x^T(t)\mathbf{P}(t-1)x(t)} \tag{10}$$

$$\mathbf{P}(t) = \mathbf{P}(t-1) - \mathbf{K}(t)x^T(t)\mathbf{P}(t-1) \tag{11}$$

where $\mathbf{K}(t)$ and $\mathbf{P}(t)$ are the gain vector and inverse covariance matrix, respectively. Moreover, the L2 regularization can be introduced by considering the initial value for $\mathbf{P}(t)$ [20]:

$$\mathbf{P}(0) = \frac{1}{\lambda}\mathbf{I} \tag{12}$$

which the cost function $J(t)$ will be penalized when large initial values of $\boldsymbol{\theta}(t)$ are considered. By applying this regularization, the numerical stability is significantly improved without modifying the recursive update structure. This formulation guarantees boundedness and smooth adaptation of the control gains in real time.

As shown in Fig. 2, the online learning mechanism is integrated into the synchronization control loop. This allows the hierarchical control system to function without the need for changes in topology. This approach improves the responsiveness and robustness of the synchronization loop, ensuring smooth transient performance, and reducing frequency mismatch among interconnected networked MGs.

Algorithm 1 presents the pseudo-code for the proposed ASCM.

Algorithm 1 Pseudo-Code of the proposed ASCM

1: **Initialize:** $\boldsymbol{\theta}(0) = [K_p^{\text{sync}}(0), K_i^{\text{sync}}(0)]^T$, $\mathbf{P}(0) = \frac{1}{\lambda}\mathbf{I}$
2: **for** each control time step t **do**
3: Measure error $e(t) = V_g \times V_{VSI}$ and integral of error $\int_0^t e(\tau)d\tau$
4: Set input vector $x(t) = [e(t), \int_0^t e(\tau)d\tau]^T$
5: Predict control output: $\hat{u}(t) = \boldsymbol{\theta}^T(t-1)x(t)$
6: Compute prediction error: $e_u(t) = u(t) - \hat{u}(t)$
7: Update gain vector:

$$\mathbf{K}(t) = \frac{\mathbf{P}(t-1)x(t)}{1 + x^T(t)\mathbf{P}(t-1)x(t)}$$

$$\boldsymbol{\theta}(t) = \boldsymbol{\theta}(t-1) + \mathbf{K}(t)e_u(t)$$

8: Update inverse covariance matrix:

$$\mathbf{P}(t) = \mathbf{P}(t-1) - \mathbf{K}(t)x^T(t)\mathbf{P}(t-1)$$

9: **end for**

B. Computational Efficiency and Transient Response Enhancement

The online ridge regression update law introduced in (9) involves only a few scalar operations and one matrix–vector multiplication, since $x(t)$ contains only the instantaneous synchronization error and its integral. As a result, the computational cost of each update will be essentially fixed at every time step. This stands in contrast to methods such

as model predictive control or reinforcement-learning-based approaches, which typically rely on iterative optimization or high-dimensional value updates that demand noticeably higher computational effort.

Moreover, as the ridge-regression mechanism increases $K_p^{\text{sync}}(t)$ and $K_i^{\text{sync}}(t)$ in proportion to the observed tracking error, the effective damping becomes time-varying and naturally strengthens when the system encounters disturbances, load changes, or PnP actions. This results in a faster drop in the error and a lower overshoot, which aligns with the boundedness properties established through the Lyapunov argument in the following subsection. Additionally, at steady state, the regularization term $\lambda|\boldsymbol{\theta}(t)|^2$ prevents the gains from drifting and maintains well-behaved adaptation while incurring a low computational cost.

C. Stability Analysis of the Adaptive Synchronization Control

To evaluate the closed-loop stability of the proposed ASCM, a Lyapunov-based approach is employed. As previously introduced in the control loop section, the adaptive controller relies on a recursive regularized least-squares estimator, where the parameter vector $\boldsymbol{\theta}(t)$, inverse covariance matrix $\mathbf{P}(t)$, and cost function $J(t)$ regulate the real-time adaptation of the controller's gains. Let $e(t)$ denote the synchronization error, defined as the phase deviation between the VSI output voltage and the corresponding MG bus voltage in the α–β frame. The control action $u(t)$, which generates the correction frequency ω_{sync}, is formulated as:

$$u(t) = K_p^{\text{sync}}(t)\, e(t) + K_i^{\text{sync}}(t) \int_0^t e(\tau)\, d\tau \tag{13}$$

$$= \boldsymbol{\theta(t)}^T \boldsymbol{x}(t) \tag{14}$$

where, as introduced earlier, $x(t) = [e(t), \int_0^t e(\tau)d\tau]$ is the regressor vector comprising instantaneous and integral synchronization errors.

To analyze the convergence behavior of this adaptive loop, the below Lyapunov candidate function can be considered [21]:

$$V(t) = \frac{1}{2}e^2(t) + \frac{1}{2\gamma}\left\|\boldsymbol{\theta}(t) - \boldsymbol{\theta}^*\right\|^2 \tag{15}$$

where $\boldsymbol{\theta}^*$ denotes the optimal controller gains and $\gamma > 0$ is a design constant. The time derivative of $V(t)$ can be obtained as follows:

$$\dot{V}(t) = e(t)\dot{e}(t) + \frac{1}{\gamma}\left(\boldsymbol{\theta}(t) - \boldsymbol{\theta}^*\right)^T \dot{\boldsymbol{\theta}}(t) \tag{16}$$

By considering the control input $u(t)$ as formulated in (14) and the error dynamics that is induced by this adaptive law, the synchronization error dynamics can be approximated as:

$$\dot{e}(t) = -\alpha e(t) + \eta(t) \tag{17}$$

where $\alpha > 0$ is a convergence rate constant and $\eta(t)$ represents bounded perturbations arising from adaptation delays or regularization effects.

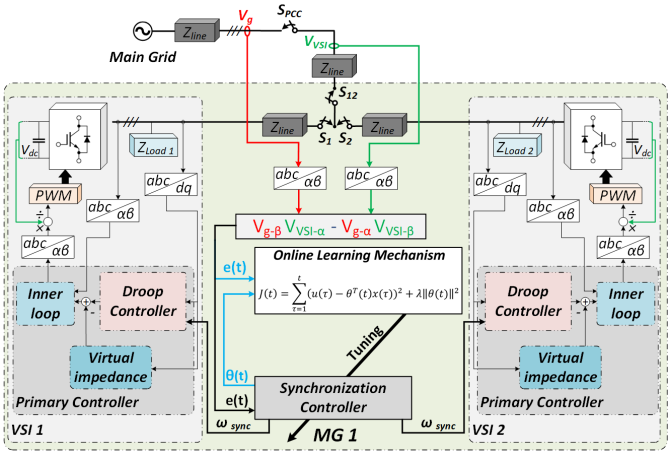

Fig. 2. The proposed Adaptive Synchronization Control Block Diagram.

By substituting (17) into (16), the Lyapunov derivative can be obtained as:

$$\dot{V}(t) = e(t)(-\alpha e(t) + \eta(t)) + \frac{1}{\gamma}\left(\boldsymbol{\theta}(t) - \boldsymbol{\theta}^*\right)^T \dot{\boldsymbol{\theta}}(t) \tag{18}$$

$$= -\alpha e^2(t) + e(t)\eta(t) + \underbrace{\frac{1}{\gamma}\left(\boldsymbol{\theta}(t) - \boldsymbol{\theta}^*\right)^T \dot{\boldsymbol{\theta}}(t)}_{\text{Bounded Adaptation Term}} \tag{19}$$

Due to the presence of L2 regularization in the gain update law, the adaptation term can be assumed to be bounded, leading to the derivation of the following inequality:

$$\dot{V}(t) \leq -\alpha\left\|e(t)\right\|^2 + \delta \tag{20}$$

where $\alpha > 0$ and $\delta > 0$ are constants that represent the convergence rate coefficient and the residual error from regularization and adaptation delay, respectively. This inequality ensures that the synchronization error $e(t)$ is uniformly ultimately bounded (UUB) and that the controller gains converge to a bounded neighborhood of their operating points [21], [22]. Furthermore, as mentioned earlier, having L2 regularization in the design ensures robustness to noise and prevents parameter drift [20]. Therefore, the closed-loop adaptive control system maintains bounded tracking error and exhibits guaranteed stability under varied operating conditions.

IV. Simulation Results

In this section, several simulation scenarios are considered, such as voltage-reference deviations, abrupt load changes, PnP operations, measurement noise, and disturbances in the communication links, to assess how the proposed secondary control system with adaptive mechanisms behaves in comparison with the conventional centralized and fixed-gain decentralized controllers. Each scenario is used to show how the adaptive learning mechanism affects the system response under the conditions noted above.

The networked ACMG setup used in the simulations is shown in Fig. 1. It consists of two MG clusters, each equipped with several VSIs and local loads. The layout includes MG units placed at different locations, each with its own load level

TABLE I
ELECTRICAL AND LINE PARAMETERS OF THE TESTBED ACMG

Parameter	Value
Filter resistance R_f (all VSIs)	0.02 Ω
Filter inductance L_f (all VSIs)	1.8 mH
DC-link capacitance C_{dc} (all VSIs)	500 μF
$Z_{line\ 12}$ (VSI 1 to VSI 2)	$R = 0.3\ \Omega$, $L = 1.8$ mH
$Z_{line\ 21}$ (VSI 2 to VSI 1)	$R = 0.4\ \Omega$, $L = 1.8$ mH
$Z_{line\ 34}$ (VSI 3 to VSI 4)	$R = 0.6\ \Omega$, $L = 1.8$ mH
$Z_{line\ 43}$ (VSI 4 to VSI 3)	$R = 0.9\ \Omega$, $L = 1.8$ mH
Interconnecting line MG 1–MG 2	$R = 0.4\ \Omega$, $L = 1.8$ mH

TABLE II
LOCAL AND DISTURBANCE LOAD PARAMETERS

Load	P (kW)	Q (kVAr)
Z_{Load1} (VSI 1)	5.5	0.5
Z_{Load2} (VSI 2)	3.5	0.7
Z_{Load3} (VSI 3)	6.5	0.6
Z_{Load4} (VSI 4)	4.5	0.3
L_{dist1} (MG 1)	10	0
L_{dist2} (MG 2)	15	0

and generation capacity, ensuring the model reflects different variations to be more realistic and closer to practice. This testbed can be extended to a larger number of clusters to reflect scalable deployments.

Tables I and II summarize the main electrical and load parameters of the understudied testbed ACMG system.

It should be mentioned that although the test system used here is scaled to the kW range for laboratory work, the same proposed adaptive control approach can be applied to MW-level systems due to its decentralized schemes and the reasonable computational cost. However, scaling up to the MW level brings a number of practical issues that are not present in smaller setups. These include longer communication delays, stronger line-impedance effects, limitations in inverter and filter design at higher power ratings, and tighter phase-synchronization requirements when MG clusters are in different geographical areas. These issues can be handled in several ways. For example, by using local synchronization buffers to compensate for data delay, employing high-precision phasor measurement units for improved frequency estimation, and adjusting the controller bandwidth or sampling frequency to account for the inertia of larger systems. A more complete assessment of these effects will be carried out through large-scale HIL experiments in future work.

All simulations scenarios were carried out in MATLAB/Simulink R2024a using the Simscape Electrical toolbox. A multi-time-scale simulation setup was adopted to balance numerical accuracy with computation efficiency. The droop control and communication layers were simulated with a discrete-time step of 50 μs, while the inner voltage and current loops used a lower time step of 10 μs to resolve the inverter dynamics. The online ridge-regression update for the adaptive synchronization controller ran asynchronously with a 1 ms update interval, which provided a practical compromise between responsiveness and computational effort.

The proposed ASCM for adaptive synchronization between MG units is implemented by using an online ridge regression algorithm, represented in Algorithm 1, which continuously updates the gains of the synchronization controller in real time. At each time step, the ASCM receives $e(t)$ and $\int_0^t e(\tau)d\tau$, and uses these inputs to update the parameter vector $\boldsymbol{\theta}(t) = [K_p^{\text{sync}}(t), K_i^{\text{sync}}(t)]^T$, without the need for intensive offline tuning or global communication. All required input data are measured locally in real time via embedded sensors in each MG unit.

A. Case Study 1 - Centralized Secondary Control System

This case study considers a simplified version of an interconnected ACMG, which is represented in Fig. 1, for evaluation. In this case study, only one VSI (VSI 1 in MG 1 and VSI 3 in MG 2) is considered for each MG system. These two MG units are connected to two different local loads (Z_{Load1} and Z_{Load2}). In this case study, to have the centralized secondary control block in the loop, $SW_{C1,b}$, $SW_{C2,b}$, $SW_{C3,b}$, and $SW_{C4,b}$ switches should be closed.

The primary and secondary controllers are added to the control loop at different times (the primary controller is connected from the beginning of the simulation test) to investigate their effect on the output voltage. As it can be seen in Fig. 3, the primary controller has difficulty reaching the voltage reference before the secondary control is added to the control loop at $t = 5s$. By having the secondary control in the loop, the output voltage is restored to the voltage reference within 2 seconds, and also reduces the steady-state error to zero.

At $t = 22s$, MG 1 and MG 2 experience fluctuations in both frequency and output voltage when a load disturbance is added (SW_{DIS} is closed). This load disturbance is disconnected at $t = 27s$, which poses a significant challenge to each MG controller (SW_{DIS} is opened). The primary challenge is to ensure that the performance of the system remains within the acceptable region by generating sufficient power despite the disturbance of the load.

Furthermore, at $t = 15s$, the connection between MG 1 and MG 2 added some voltage and system frequency fluctuations (SW_1, SW_3, SW_{12}, and SW_{34} are closed). The simulation results depicted in Fig. 3 show that the centralized droop-based control system is successful in regulating the output voltages and system frequency in various simulation scenarios. However, the system's performance can still be improved in terms of faster response to voltage reference and local loads deviation that may be computationally expensive to address with centralized control schemes. The centralized controller might also cause single-point failure issues. However, this approach ensured compliance with relevant MG standards [13] and demonstrated satisfactory performance in maintaining the stability and reliability of the MG system.

B. Case Study 2 - Proposed Adaptive Decentralized Secondary Control System

In this case study, as depicted in Fig. 1, the ACMG system comprises two MG systems with two VSIs in each (VSI 1, VSI 2 in MG 1 and VSI 3, VSI 4 in MG 2). These two MG systems are connected to four different local loads (Z_{Load1},

This article has been accepted for publication in IEEE Transactions on Industry Applications. This is the author's version which has not been fully edited and content may change prior to final publication. Citation information: DOI 10.1109/TIA.2026.3654503

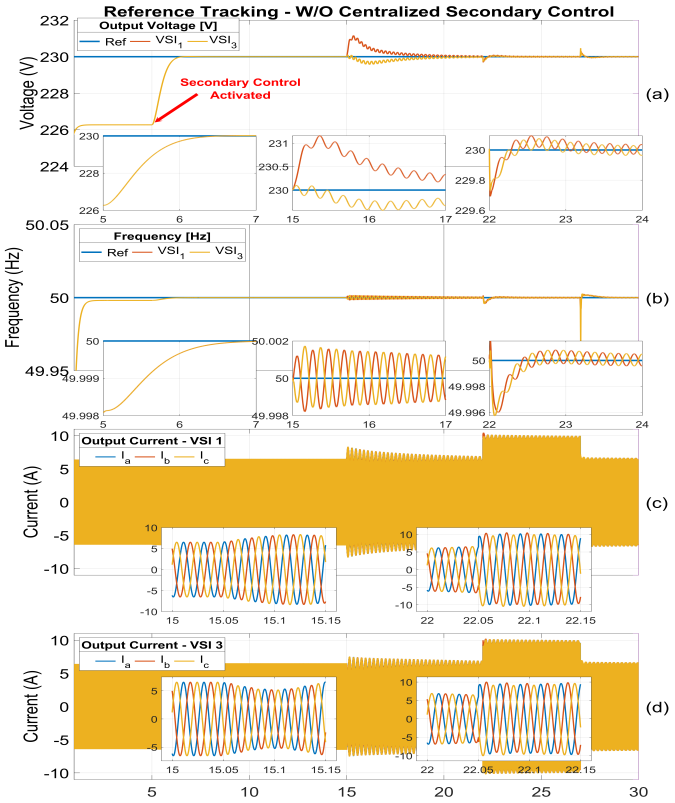

Fig. 3. System Performance Under Voltage Reference and Load Deviations - With and Without Centralized Secondary Control System.

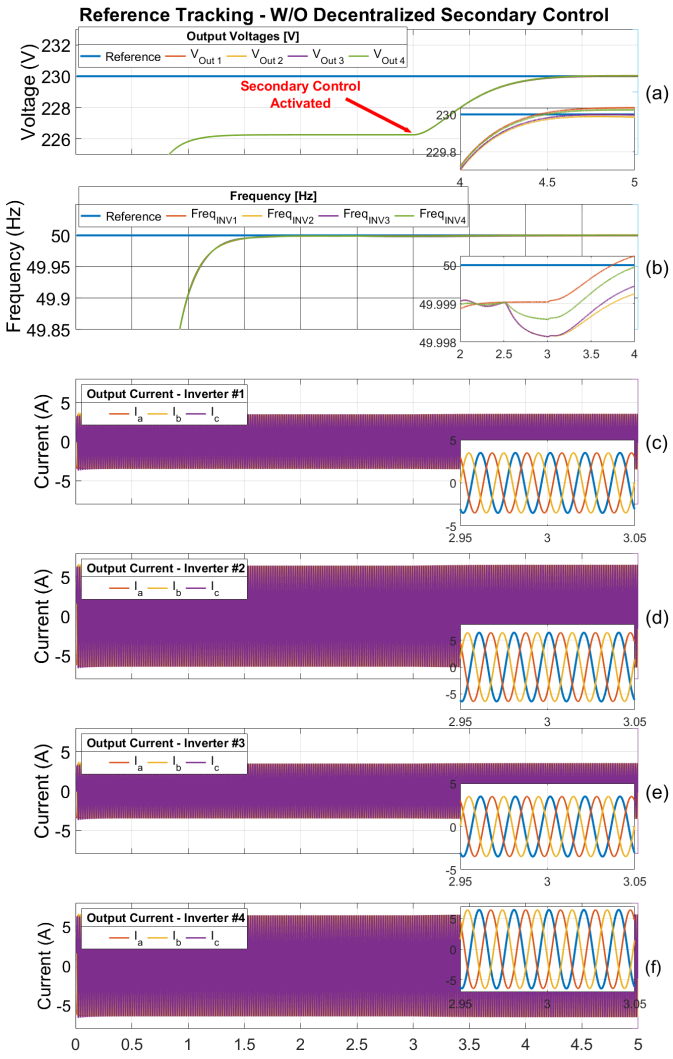

Fig. 4. System Performance with and without a Decentralized Secondary Control System.

Z_{Load2}, Z_{Load3} and Z_{Load4}). In this case study, to have the decentralized secondary control block in the loop, $SW_{C1,a}$, $SW_{C2,a}$, $SW_{C3,a}$, and $SW_{C4,a}$ switches should be closed.

As previously discussed in Case study 1, the primary and secondary controllers are added into the control loop at different time intervals to assess their impact on the output voltage. Similar to the results for the centralized architecture, the primary controller faces challenges in tracking the voltage reference without the assistance of the secondary control. At $t = 3s$, the secondary controller is added to the control loop. Having the secondary controller in the control loop facilitates the output voltage tracking operation, as can be seen from Fig. 4, each unit's output voltage can rapidly track voltage reference deviations within less than half a second and also effectively reduces the steady-state error to zero. This is a significant improvement, surpassing the centralized control by 1.5 seconds, as shown in Fig. 3, which shows that the proposed decentralized control achieves a 75% reduction in response time to rapid voltage reference changes.

1) Voltage Deviation Handling: The decentralized control system is designed to be highly responsive to voltage deviations within each MG unit at different intervals. In other words, the secondary controller must generate different voltage references for each primary control unit of each MG systems to maintain the specific rated power generation while accounting for different load profiles and power generation capacities, as most units rely on renewable-based power generation. This reference tracking capability is critical to the system's design and must be evaluated in various scenarios to ensure grid stability and prevent disruptions caused by voltage fluctuations.

For this purpose, at specific time intervals ($t = 19$, 23, 26, and 29 seconds), a ±2-volt voltage disturbance is introduced to the voltage references of VSIs 1, 2, 3, and 4 as can be seen in Fig. 5. Although these voltage deviations could have destabilized the whole MG system and caused potential disruptions, the proposed decentralized control mechanism can efficiently detect and respond to these voltage fluctuations quickly (less than half a second compared to 2 seconds with centralized control in the loop).

2) Load Changes: In this case study, the performance of the ACMG system is evaluated under several sudden load changes in both the local and common loads. To test this, as shown in Fig. 6, the model incorporated various load disturbances at different time intervals. Several load disturbances are introduced at two different time intervals: $t = [35, 37]$ (SW_{DIS1} closed at $t = 35s$ and opened at $t = 37s$) and $t = [39, 41]$ (SW_{DIS2} closed at $t = 39s$ and opened at $t = 41s$). As can be seen in Fig. 6, the system is completely capable of

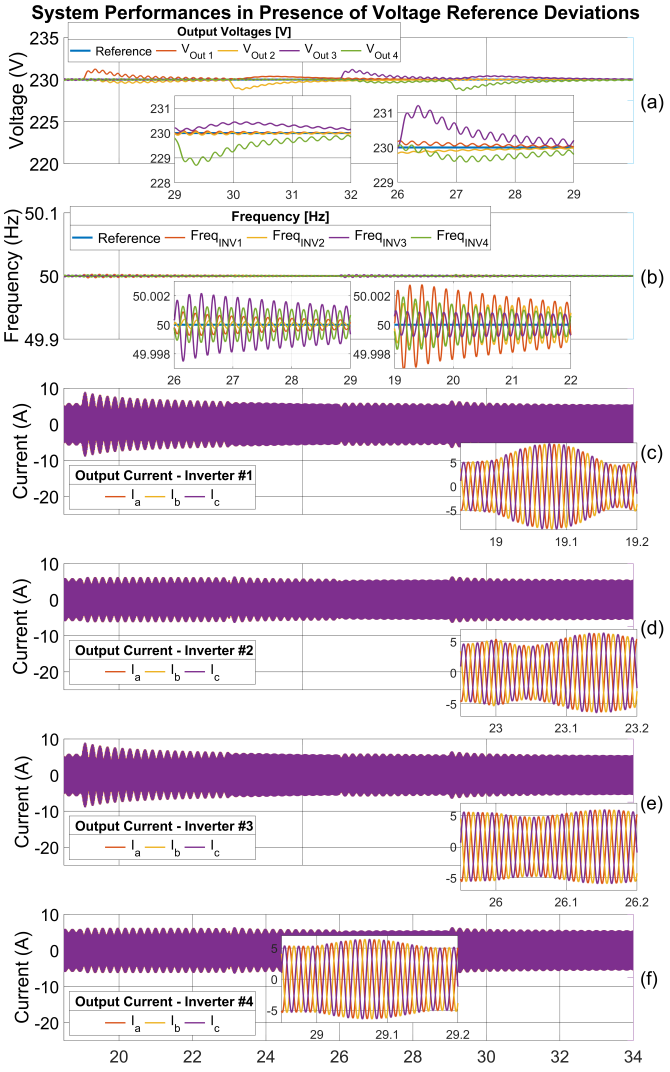

Fig. 5. System Performance Under Different Rapid Voltage Reference Deviation.

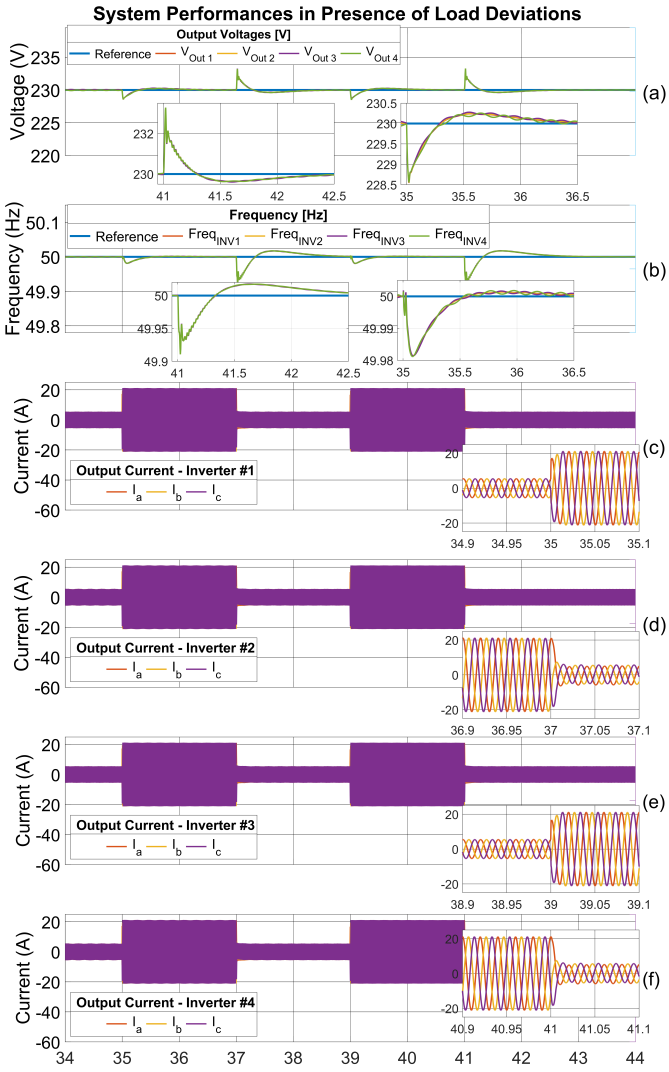

Fig. 6. System Performance Under Different Abrupt Load Deviations.

responding to these load disturbances, demonstrating its ability to handle these fluctuations in demand and maintain a stable power supply.

3) Plug-and-Play Functionality: In this case study, the PnP functionality for the MG test bed is considered. Detailed coordination is required to manage the PnP functionality between interconnected MGs. To facilitate this, the secondary control system including the synchronization control system (depicted in Fig. 2) play a critical role in ensuring seamless management of unit connections and disconnections. By synchronizing frequency and voltage, MGs can achieve seamless connection and provide a stable and reliable power supply to connected loads. This study analyzes the output voltage and system frequency responses of four VSI units: VSI 1, VSI 2, VSI 3, and VSI 4 in the understudied MG system with two different synchronization control systems. The main focus of this case study is to investigate the performance of these units and their ability to maintain stable voltage and frequency levels under varying operating conditions. The results of this analysis will provide valuable information on the design and operation of MG systems, which are increasingly important for ensuring the resilience and reliability of the power grid. Fig. 7 and Fig. 8 show the performance of the system with the conventional synchronization control system and the ASCM in the loop, respectively. As shown, at different times, VSI 1 is connected to VSI 2, VSI 3 is connected to VSI 4, and MG 1, which consists of VSI 1&2 is connected to MG 2, which consists of VSI 3&4 at $t = 6$ (SW_1 and SW_2 closed), $t = 10$ (SW_3 and SW_4 closed), and $t = 13$ (SW_{12} and SW_{34} closed), respectively. As shown in Fig. 8, the performance of the system is significantly improved by having an online adaptive synchronization mechanism in the loop. For example, the system frequency deviation during the unit PnP functionality is approximately 10 times attenuated (from ±0.01 Hz to ±0.001 Hz). This synchronized coordination increases the stability and reliability of the MG system and realizes PnP operation.

4) Robustness to Measurement Noise and Packet Loss: To evaluate the robustness of the proposed adaptive control framework, random Gaussian measurement noise with an SNR of 40 dB is added to the voltage and frequency signals, and random packet dropouts (up to 10%) are introduced in

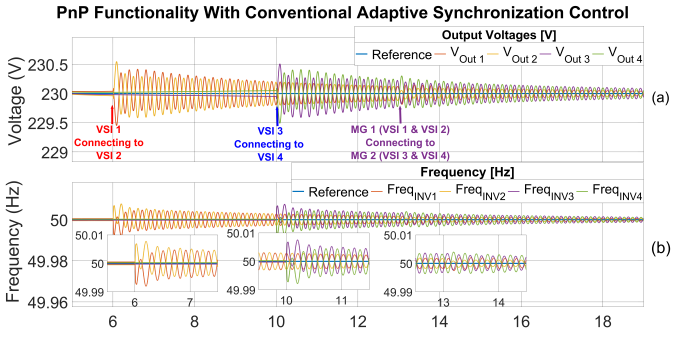

Fig. 7. PnP Performance of Microgrid Units Using a Conventional Synchronization Control.

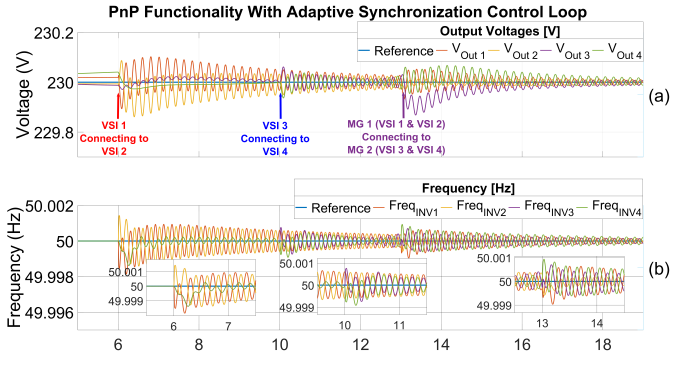

Fig. 8. PnP Performance of Microgrid Units Using the Proposed ASCM.

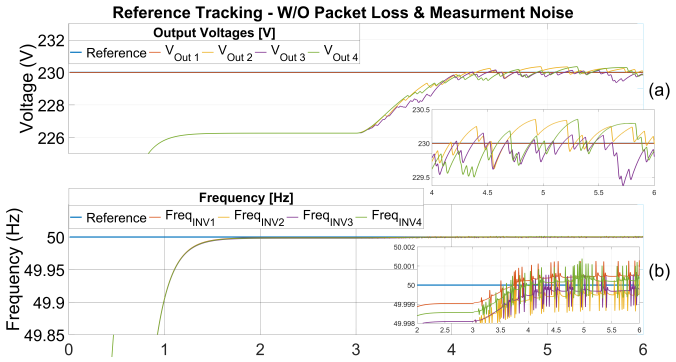

Fig. 9. System Performance Under Measurement Noise and 10% Packet Loss.

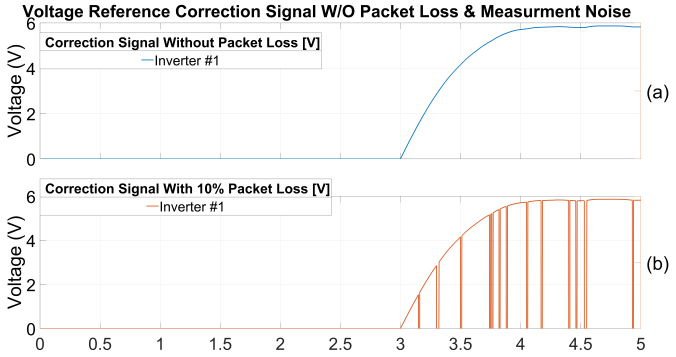

Fig. 10. Secondary Control Reference Correction Signal with and without Measurement noise and 10% Packet Loss.

the communication links between the secondary and primary control layers. The results show that the adaptive ridge-regression-based estimator maintains convergence and smooth gain adaptation, with less than 2.5% deviation in steady-state error compared to the ideal case. The L2 regularization term λ effectively suppresses the impact of noisy measurements, confirming the robustness of the proposed control under imperfect communication conditions. As shown in Fig. 9, the output voltages of all four VSI units are still able to track their reference values despite the presence of 40 dB measurement noise and 10% packet loss. Furthermore, Fig. 10 illustrates the corresponding secondary control reference correction signal for a representative unit, where the chattering caused by random packet loss does not compromise overall stability or tracking performance.

V. Discussion

Overall, the proposed adaptive secondary control shows a clear advantage over both the conventional centralized and the fixed-gain decentralized control systems. The controller reacts quickly to voltage deviations and load changes, and it also handles PnP events reliably even when measurement noise or packet loss is present. This helps maintain stable functionality among the MG clusters without relying on strong and reliable communication links.

The quantitative results in Table III provide a comprehensive comparison using three standard metrics: Ts (settling time), OS (percentage overshoot), and SSE (steady-state error). In all conducted simulation scenarios, the proposed adaptive control delivers the smallest tracking error and the fastest settling. For instance, in Case 1 (voltage reference deviation), the settling time decreases from 2s with centralized control and 1.4s with the fixed-gain decentralized method to only 0.5s. A similar situation is also seen under load disturbances (Case 2), where the adaptive controller settles in 0.8s.

PnP events (Case 3) normally create a larger transient response, although the adaptive controller still converges in 1.1s, noticeably faster than centralized control. The effect of the online learning mechanism becomes even more obvious in Case 4, where both measurement noise and packet loss are introduced. Here, the centralized method becomes unstable, and the fixed-gain decentralized controller recovers more slowly and with larger errors. In contrast, the adaptive approach remains stable, with a settling time of 0.7s and a steady-state error of 2.1%. This indicates that the ridge-regression update provides adequate damping and smooth gain adjustment even under imperfect communication. These observations highlight the improvements in transient response, tracking accuracy, and disturbance tolerance offered by the proposed method.

Although conventional decentralized and centralized controllers may still work in applications with modest performance requirements, systems that depend on tight coordination, such as electric ships, data centers, or remote power systems, benefit more from the adaptive synchronizing layer. Several results illustrate this: Figs. 3, 5 and 6 show shorter response times during voltage deviations, Fig. 4 shows that the voltage reference is reached in 0.5s rather than the 1.5s required under centralized control, and Figs. 7 and 8 show that frequency deviations during PnP are reduced (∼10×) with the

TABLE III
QUANTITATIVE PERFORMANCE COMPARISON UNDER VOLTAGE REFERENCE DEVIATIONS, LOAD, AND COMMUNICATION DISTURBANCES

Case Study	Centralized			Conventional Decentralized			Proposed Method		
	Ts (s)	OS (%)	SSE (%)	Ts (s)	OS (%)	SSE (%)	Ts (s)	OS (%)	SSE (%)
Case 1: Voltage reference deviation	2.0	8.2	1.5	1.4	6.7	1.2	**0.5**	**2.1**	**0.11**
Case 2: Load step	2.4	7.8	2.2	1.9	6.9	1.8	**0.8**	**2.3**	**0.15**
Case 3: Plug-and-play event	2.8	9.9	3.1	2.6	7.4	2.5	**1.1**	**3.1**	**0.27**
Case 4: 40 dB Noise + 10% Packet Loss		Unstable		5.9	9.0	8.5	**0.7**	**2.5**	**0.36**

proposed adaptive strategy.

VI. CONCLUSION AND FUTURE WORK

This study introduced an online ASCM for networked ACMG systems. The method relies on an online ridge-regression learning rule that operates as a Bayesian-style update for the synchronization control loop. Across the simulation studies, the controller with the proposed adaptive mechanism showed clear improvements compared with the conventional centralized and decentralized (fixed-gain) approaches used as benchmarks. In particular, the adaptive secondary layer reacted more quickly to voltage-reference deviations and load changes, and it restored the system operating point after disturbances with noticeably less delay. In addition, the automatic gain adjustment provides a practical level of flexibility during dynamic operating conditions, without relying on global communication channels or heavy offline tuning. As the future steps for the continuation of this work, full-scale HIL testing will be carried out using the real-time setup. Additionally, a comprehensive systematic comparison with other adaptive or data-driven synchronization strategies under more demanding and realistic operating conditions, including larger network sizes and stronger uncertainties, will be conducted by the authors. These directions will help clarify how the proposed ASCM behaves in practical deployments and where it stands relative to other emerging techniques.

ACKNOWLEDGMENT

This work was supported by VILLUM FONDEN, Denmark, under the VILLUM Investigator Grant (no. 25920); Center for Research on Microgrids (CROM).

REFERENCES

[1] M. I. Saleem, S. Saha, U. Izhar, and L.-m. Ang, "Integration challenges of inverter based renewable energy sources in weak grids," in *2022 IEEE Industry Applications Society Annual Meeting (IAS)*. IEEE, 2022, pp. 1–18.

[2] A. Basati, J. M. Guerrero, J. C. Vasquez, A. Fakharian, K. H. Johansson, and S. Golestan, "Robust internal model-based voltage control for dc microgrids: An lmi based $h\,\mathrm{inf}$ control," *Sustainable Energy, Grids and Networks*, vol. 35, p. 101094, 2023.

[3] A. Basati, "Cyber-resilient control structures in dc microgrids with cyber-physical threats," 2023.

[4] A. Basati, J. M. Guerrero, J. C. Vasquez, N. Bazmohammadi, and S. Golestan, "A data-driven framework for fdi attack detection and mitigation in dc microgrids," *Energies*, vol. 15, no. 22, p. 8539, 2022.

[5] A. Basati, J. Wu, J. M. Guerrero, and J. C. Vasquez, "Internal model-based voltage control for dc microgrids under unknown external disturbances," in *2022 International Conference on Smart Energy Systems and Technologies (SEST)*. IEEE, 2022, pp. 1–6.

[6] J. M. Guerrero, J. C. Vasquez, J. Matas, L. G. De Vicuña, and M. Castilla, "Hierarchical control of droop-controlled ac and dc microgrids—a general approach toward standardization," *IEEE Transactions on industrial electronics*, vol. 58, no. 1, pp. 158–172, 2010.

[7] J. C. Vasquez, J. M. Guerrero, M. Savaghebi, J. Eloy-Garcia, and R. Teodorescu, "Modeling, analysis, and design of stationary-reference-frame droop-controlled parallel three-phase voltage source inverters," *IEEE Transactions on industrial electronics*, vol. 60, no. 4, pp. 1271–1280, 2012.

[8] A. Basati, N. Bazmohammadi, Y. Guan, J. C. Vasquez, and J. M. Guerrero, "Resilience oriented distributed secondary control for networked microgrids: A case study from indonesia," pp. 512–517, 2024.

[9] N. Mohammed, A. Lashab, M. Ciobotaru, and J. M. Guerrero, "Accurate reactive power sharing strategy for droop-based islanded ac microgrids," *IEEE Transactions on Industrial Electronics*, vol. 70, no. 3, pp. 2696–2707, 2022.

[10] J. M. Guerrero, M. Chandorkar, T.-L. Lee, and P. C. Loh, "Advanced control architectures for intelligent microgrids—part i: Decentralized and hierarchical control," *IEEE Transactions on Industrial Electronics*, vol. 60, no. 4, pp. 1254–1262, 2012.

[11] H. Han, X. Hou, J. Yang, J. Wu, M. Su, and J. M. Guerrero, "Review of power sharing control strategies for islanding operation of ac microgrids," *IEEE Transactions on Smart Grid*, vol. 7, no. 1, pp. 200–215, 2015.

[12] N. Modig, R. Eriksson, P. Ruokolainen, J. N. Ødegård, S. Weizenegger, and T. D. Fechtenburg, "Overview of frequency control in the nordic power system," *Nordic Analysis Group*, 2022.

[13] "Ieee standard for interconnection and interoperability of distributed energy resources with associated electric power systems interfaces," *IEEE Std 1547-2018 (Revision of IEEE Std 1547-2003)*, pp. 1–138, 2018.

[14] Z. Lian, C. Wen, F. Guo, P. Lin, and Q. Wu, "Decentralized secondary control for frequency restoration and power allocation in islanded ac microgrids," *International Journal of Electrical Power & Energy Systems*, vol. 148, p. 108927, 2023.

[15] J. M. Guerrero, J. C. Vasquez, J. Matas, L. G. De Vicuña, and M. Castilla, "Hierarchical control of droop-controlled ac and dc microgrids—a general approach toward standardization," *IEEE Transactions on industrial electronics*, vol. 58, no. 1, pp. 158–172, 2010.

[16] Q. Shafiee, J. M. Guerrero, and J. C. Vasquez, "Distributed secondary control for islanded microgrids—a novel approach," *IEEE Transactions on Power Electronics*, vol. 29, no. 2, pp. 1018–1031, 2014.

[17] S. Golestan, J. M. Guerrero, and J. C. Vasquez, "Three-phase plls: A review of recent advances," *IEEE Transactions on Power Electronics*, vol. 32, no. 3, pp. 1894–1907, 2017.

[18] B. Priyanka, M. Lavanya *et al.*, "Phase-locked loop (pll) techniques for grid synchronization: A comprehensive review," in *2024 Second International Conference on Emerging Trends in Information Technology and Engineering (ICETITE)*. IEEE, 2024, pp. 1–9.

[19] C. Cortes, M. Mohri, and A. Rostamizadeh, "L2 regularization for learning kernels," *arXiv preprint arXiv:1205.2653*, 2012.

[20] R. Ouhamma, O.-A. Maillard, and V. Perchet, "Stochastic online linear regression: the forward algorithm to replace ridge," in *Advances in Neural Information Processing Systems*, M. Ranzato, A. Beygelzimer, Y. Dauphin, P. Liang, and J. W. Vaughan, Eds., vol. 34. Curran Associates, Inc., 2021, pp. 24 430–24 441. [Online]. Available: https://proceedings.neurips.cc/paper_files/paper/2021/file/cca289d2a4acd14c1cd9a84ffb41dd29-Paper.pdf

[21] H. K. Khalil, "Lyapunov stability," *Control systems, robotics and automation*, vol. 12, p. 115, 2009.

[22] S. Yuan, M. Lv, S. Baldi, and L. Zhang, "Lyapunov-equation-based stability analysis for switched linear systems and its application to switched adaptive control," *IEEE Transactions on Automatic Control*, vol. 65, no. 12, pp. 5233–5240, 2020.

Amir Basati (Member, IEEE) received the B.Sc. degree in Electrical Engineering – Biomedical Systems in 2012, the M.Sc. degree in Electrical Engineering – Control Systems in 2016, and the Ph.D. degree in AI-based control for cyber-physical energy systems in 2023. He is currently a Postdoctoral Researcher with the Center for Research on Microgrids (CROM), AAU Energy, Aalborg University, Denmark. His research interests include control and optimization of power converters, electric drives, and microgrids; cyber-physical security and resilient control; networked and distributed control systems; and data-driven and digital-twin-based methods for energy applications.

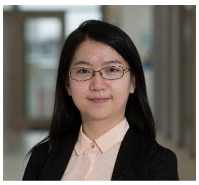

Yajuan Guan (Member, IEEE) received the B.S. degree and M.S. degree in electrical engineering from Yanshan University, Qinhuangdao, Hebei, China, and the Ph.D. degree in power electronics from the Aalborg University (AAU), Aalborg, Denmark, in 2007, 2010 and 2016 respectively. From 2010 to 2013, she was a Research Intern and then an Assistant Researcher at the Institute of Electrical Engineering, Chinese Academy of Sciences. From 2016 to 2022, she was a postdoctoral Fellow and then an Assistant Professor at Center for Research on Microgrids (CROM), AAU. She is currently an Associate Professor at CROM, AAU. Her research interests include microgrids, distributed generation systems, power converters for renewable energy generation systems, Internet of Things, grid-forming wind power systems, power supply resilience, and maritime microgrids.

Najmeh Bazmohammadi (Senior Member, IEEE) received a B.Sc. degree in Electrical Engineering and the M.Sc. degree in Electrical Engineering- Control theory in 2009 and 2012, respectively, and a Ph.D. degree in Electrical Engineering- Control theory in 2019. She is currently an Assistant Professor with the Center for Research on Microgrids, AAU Energy, Aalborg University, Denmark. Her current research interests include modeling, optimization, and energy management of hybrid and renewable-based Microgrids, model predictive control, digital twins, and system dynamics.

Juan C. Vasquez (Senior Member, IEEE) received both B.Sc. and M.Sc. degrees from UAM, Colombia, and Ph.D. degrees from UPC, Spain. In 2019, he became a Professor in Sustainable and Resilient Microgrids. Currently, he is the acting director of the Center for Research on Microgrids. He has published more than 650 journal articles, which have been cited more than 45500 times. He has been a Highly Cited Researcher, since 2017, and was a recipient of the Young Investigator Award, in 2019.

Josep M. Guerrero (Fellow, IEEE) received the B.Sc., M.Sc., and the Ph.D. degrees in power electronics from the Technical University of Catalonia, Barcelona, in 1997, 2000 and 2003, respectively. Prof. Guerrero is a Villum Investigator by the Villum Fonden, which supports the Center for Research on Microgrids. He is a full professor with AAU Energy, Aalborg University, Denmark, and is a research Professor at the Catalin Institution for Research and Advanced Studies with the Technical University of Catalonia, Spain. His research interests are oriented toward different microgrid frameworks.